Ionics
https://doi.org/10.1007/s11581-018-2757-2

ORIGINAL PAPER

Ordering and diffusion in liquid magnesium antimonide (Mg_3Sb_2) from hypernetted-chain theory and molecular dynamics simulation

Ünsal Akdere[1] · Seçkin D. Günay[1] · Çetin Taşseven[1]

Received: 10 April 2018 / Revised: 30 September 2018 / Accepted: 4 October 2018
© Springer-Verlag GmbH Germany, part of Springer Nature 2018

Abstract

The static structure and ionic transport in molten Mg_3Sb_2 was investigated by means of the hypernetted-chain theory of liquids (HNC) and the molecular dynamics simulation (MD) using a semi-empirical pairwise potential together with the liquid-state density that was estimated from the procedure of finding minimum energy. Magnesium sublattice melts into a more disordered liquid state with a higher mobility compared to antimony. Highly mobile magnesium ions indicate the cluster distribution over a range. Tendency of the pre-peak at low k region ($k \cong 1.7\text{Å}^{-1}$) in the pair structure factor $S_{NN}(k)$ may be the result of the one of the n-fold Voronoi coordination polyhedral clusters that dominates over the other clusters. The results also suggest that the pair structure factor of the less mobile ion influences the low- k peak in $S_{NN}(k)$ that might be a characteristic feature of the systems whose components have markedly different self-ionic diffusion.

Keywords Liquid · Magnesium antimonide · Structure · Diffusion

Introduction

Like other magnesium pnictides, magnesium antimonide, Mg_3Sb_2, has gained substantial attraction due to its potential technological and industrial applications as a high performance thermoelectric material with a low thermal conductivity [1–4]. The liquid state of Mg_3Sb_2 has also been used as an electrolyte in the energy storage system at Massachusetts Institute of Technology (MIT), which has been called the ambipolar electrolysis cell [5]. The electronic structure, lattice dynamics, and elastic and thermal properties of Mg_3Sb_2 have been studied from the first-principles calculations, along with some other magnesium pnictides [6–9]. Thermal expansion, heat capacity, and some bulk properties have been reported by means of classical molecular dynamics (MD) simulation method with a semi-empirical classical interionic potential [10]. The setup of the ambipolar cell contains the liquid state of magnesium and antimony as the top and the bottom electrode layers, and molten salt as the electrolyte in the middle layer, all of which are immiscible liquids. This set of liquid metal electrodes and ionically conductive electrolyte operates at high temperatures (~ 1000 K) with high ion mobility, which allows a very high current flow greater than ordinary batteries. Thus, it is of great importance to study the high temperature structural ordering and transport properties of molten magnesium antimonide. The classical computer simulation method and liquid state theories (LST) are useful tools in order to estimate such physical properties of ionic liquids. In this study, we have investigated the topological ordering, chemical ordering and ionic diffusion of the molten Mg_3Sb_2 evaluated by the use of hypernetted-chain (HNC) approximation of LST and MD simulation method along with a semi-empirical rigid ion potential.

Electronic supplementary material The online version of this article (https://doi.org/10.1007/s11581-018-2757-2) contains supplementary material, which is available to authorized users.

✉ Seçkin D. Günay
sgunay@yildiz.edu.tr

[1] Department of Physics, Faculty of Science, Yıldız Technical University, Esenler, 34210 İstanbul, Turkey

Methodology and details of calculations

LST-HNC approximation

For a homogeneous and isotropic liquid system, correlation functions for ionic components i and j can be related by the well-known Ornstein-Zernike (OZ) integral equation [11],

Published online: 07 November 2018

$$\gamma_{ij}(r) \equiv h_{ij}(r) - c_{ij}(r) = \sum_l \rho_l \int d\vec{r}' c_{il}\left(|\vec{r} - \vec{r}'|\right) h_{lj}\left(\vec{r}'\right) \quad (1)$$

where $h_{ij}(r)$ and $c_{ij}(r)$ are the total and the direct correlations, respectively. Various liquid-state closures are obtained by the approximation made on direct correlation function. The HNC approximate closure for an ionic liquid can be deduced by considering only the indirect part of the exponential expansion of $c_{ij}(r)$, that is the radial distribution function $g_{ij}(r)$,

$$c_{ij}(r) = g_{ij}(r) - 1 - \frac{1}{k_B T}\phi_{ij}(r) - ln\left[g_{ij}(r)\right] \quad (2)$$

where $\phi_{ij}(r)$ is the electrostatic pair potential modeling the interionic interactions in the fluid and $g_{ij}(r) = h_{ij}(r) - 1$. The OZ integral equation has been solved numerically following the method originally proposed by Gillan [12] and Abernethy-Gillan [13], which is basically combination of Picard and Newton-Raphson methods. The method leads to an accurate solution of the OZ equation in about 20–30 iterations with initial estimation made on $\gamma_{ij}(r)$ as the solution of mean spherical approximation (MSA) [11] with charged hard-spheres. The accuracy of the solution at each stage was taken as $\left|\gamma_{ij}^{k+1}(r) - \gamma_{ij}^{k}(r)\right| < 10^{-4}$. $M = 2048$ mesh points were used for each run by cooling down the system gradually from an initial temperature T_i to the desired temperature T_f. Mesh length in real and reciprocal space are adjusted using $\Delta r \cdot \Delta k = 2\pi/M$.

MD simulation

The crystal $\alpha - Mg_3Sb_2$ has anti $- La_2O_3$ type of structure with the space group of $P\bar{3}m1$ and hexagonal unit cell axes of $a = 4.568\text{Å}$ and $c = 7.229\text{Å}$ containing one formula unit [6]. The solid-state MD cell was constructed by setting the number of Mg^{+2} and Sb^{-3} ions as 1536 and 1024, respectively, in a box of $8 \times 8 \times 8$. Calculations were carried out using the molecular dynamics simulation code called MOLDY [14]. The long-range Coulomb interactions were handled by Ewald's sum method. Direct space cut-off distance was 20 Å. The Beeman's predictor-corrector algorithm was applied to solve the Newton's equation of motion to compute the positions and velocities of the ions with the time step of $\Delta t = 1\text{fs}$. The simulations were performed in constant pressure - constant temperature (NPT) ensemble at $T = 300K$ (solid phase) and $T = 1550K$ (liquid phase). Non-isobaric ensemble is applied to the solid phase cell to allow the non-uniform dilation for each axis. Isobaric ensemble is applied to the liquid phase for the uniform dilation. At 1550 K, since magnesium antimonide is in liquid form, MD simulation box has a cubic structure in accordance with the equilibrium density. Initial configurations of atoms were determined by the skew start method [14].

Temperature rescaling method was used to keep the system at the desired temperature in the first 30 ps. When the system reaches equilibrium, rescaling is turned off. Then, the temperature is allowed fluctuating spontaneously around the desired value without any external influence. The initial run to reach the desired equilibrium state is not used for the calculation of physical properties, then the structural and transport properties were calculated by averaging over the following 470 ps.

Potential

Both the HNC theory and MD simulation calculations have been carried by modeling the interaction between ionic species with the Buckingham type of rigid ion potential of the form of [15].

$$\phi_{ij}(r) = \frac{Z_i Z_j}{r} + A_{ij} exp\left(-\frac{r}{\rho_{ij}}\right) - \frac{C_{ij}}{r^6} \quad (3)$$

The potential has been parameterized for the solid-state properties of $\alpha - Mg_3Sb_2$ where the effective charges are $Z_{Mg} = 1.322392e$, $Z_{Sb} = -1.983588e$; the strength of short-range interactions of ions is $A_{Sb-Mg} = 1300.0\ eV$, $A_{Mg-Mg} = 9547.96\ eV$, $A_{Sb-Sb} = 9045.06\ eV$; the hardness parameters are $\rho_{Sb-Mg} = 0.383333\ \text{Å}, \rho_{Mg-Mg} = 0.21916\text{Å}, \rho_{Sb-Sb} = 0.39\ \text{Å}$; van der Waals parameters are

$C_{Sb-Mg} = 94.0\ eV\text{Å}^6, C_{Mg-Mg} = 0.0 eV\text{Å}^6, C_{Sb-Sb} = 1658.102\ eV\text{Å}^6$

, which have been found to give the lattice constants and mechanical properties in fairly good agreement with the available experimental data and the first-principles calculations (Table 1). Mechanical properties have been calculated with GULP program [16].

Results and discussion

In order to execute the HNC calculation, the number density ρ of Mg_3Sb_2 at liquid phase is required as one of the input parameters. However, to the best of our knowledge, there are no data available in the literature. Therefore, we have developed the following procedure to estimate the liquid density at $T = 1550K$ from HNC approximation. Once the radial distribution functions $g_{ij}(r)$ are calculated by solving the OZ Eq. (1) in conjunction with the HNC closure (Eq. 2) and the model potential (Eq. 3), the internal energy per particle of a two component liquid can be obtained from

$$\frac{E}{N} = \frac{3}{2}k_B T + \frac{\rho}{2}\sum c_i c_j \int g_{ij}(r)\phi_{ij}(r) d^3\vec{r} \quad (4)$$

where ρ and $c_x\ (x = i, j)$ are the number density and the number concentrations, respectively. The OZ equation was solved for

Table 1 Calculated lattice constants and mechanical properties of α-Mg_3Sb_2 are compared with available data in the literature

	Exp. [17]	First-principles [6]	Present work
Lattice constant a(Å)	4.568	4.5062	4.57
c(Å)	7.229	7.1582	7.06
Bulk modulus (GPa)		48.8	48.76
Shear modulus (GPa)		22.6	12.76
C_{11} (GPa)		87.5	82.88
C_{33} (GPa)		91.9	59.75
C_{12} (GPa)		43.6	55.24
C_{13} (GPa)		21.7	33.83
C_{44} (GPa)		17.8	29.89

10 different ionic number density points varying the data between $\rho = 0.032\,ion/Å^3 - 0.041\,ion/Å^3$with the density steps of $\Delta n = 10^{-3}\,ion/Å^3$ at the constant temperature of $T = 1550\,K$. The minimum energy criterion $\left(\frac{dE}{d\rho}\right)_T = 0$ is taken to obtain equilibrium density at the desired temperature. This procedure is given in the Fig. 1 as the internal energy per ion versus total ionic number density. The equilibrium densities were estimated as $\rho(T = 1550K) = 0.03722\,ions/Å^3 = 3.911\,g/ml$. The density is reduced by 2.7% upon melting compared to the experimental solid-state density $4.02g/ml$. The solid- (300 K) and liquid-state (1550 K) densities from MD simulations were $0.0391\,ion/Å^3 = 4.109\,g/ml$ and $0.03504\,ion/Å^3 = 3.682\,g/ml$, respectively. The picture inserted in Fig. 1 is the snapshot at the equilibrium density produced by MD simulation at 1550 K. The energy-pressure and pressure-density phase diagrams are also provided as supplementary materials (Online Resource 1–2).

The radial distribution function $g_{ij}(r)$ gives the quantitative measure of the local order-disorder of the structure of binary compounds. The HNC results for the $g_{ij}(r)$ of molten Mg_3Sb_2 at $T = 1550K$ are presented in Fig. 2. The $g_{ij}(r)$ of solid Mg_3Sb_2 of MD calculation at $T = 300K$ is included for comparison. As expected, $g_{ij}(r)$ of anion and cation pairs display the characteristic features of an ionic melt.

The average nearest-neighbor principal peak positions for Sb − Mg, Mg − Mg, and Sb − Sb separations of liquid phase are 2.7 Å, 3.65 Å, and 4.30 Å, respectively, which have not significantly changed during melting. The Mg − Mg pair has less intensive principal peak and second peak than those of Sb − Sb indicating more mobile character of Mg ions compared to Sb ions. Due to the higher mobility of Mg ions and also increasing intensity of the first minima in $g_{SbMg}(r)$, the penetration of Mg ions into the first coordination shell of $Sb - Mg$

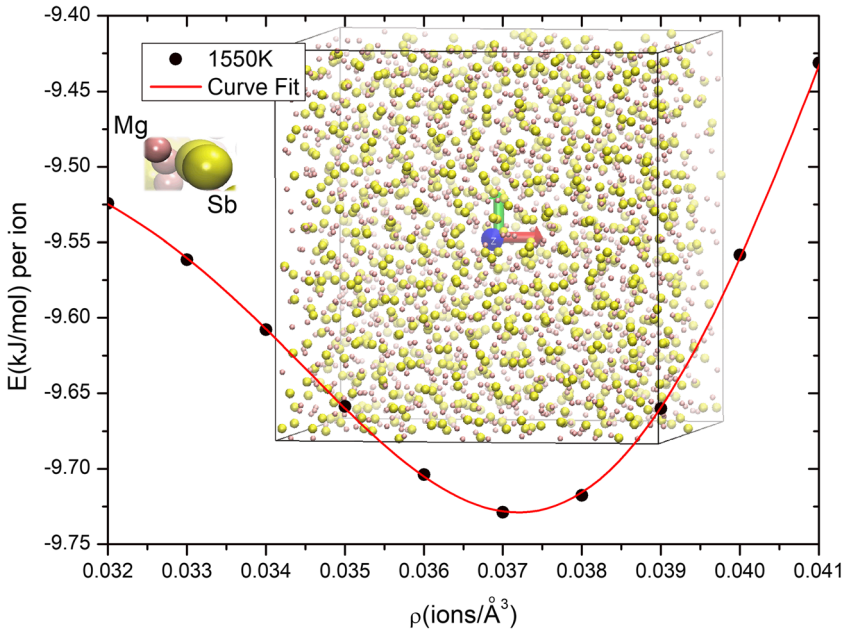


Fig. 1 The internal energy per ion versus total ionic number density at $T = 1550$ K from HNC calculation. The inset picture is the snapshot of the equilibrium density produced by MD simulation at 1550 K. 296 × 209 mm (300 × 300 DPI)

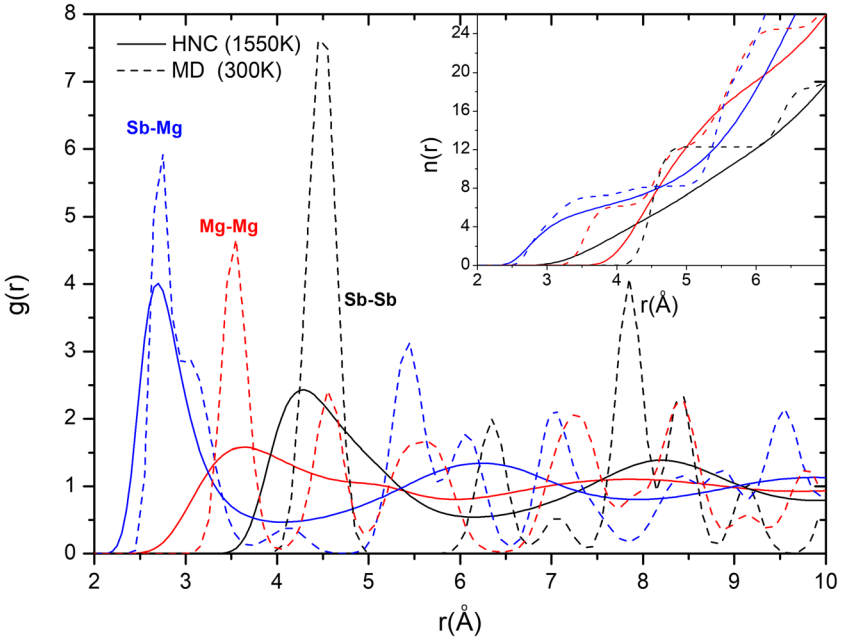


Fig. 2 The radial distribution function $g_{ij}(r)$ and the running coordination numbers $n_{ij}(r)$ of Mg_3Sb_2 at T = 1550 K (liquid phase) from the HNC theory and T = 300 K (solid phase) from MD simulation. 291 × 203 mm (300 × 300 DPI)

pairs is observed, as a result of which the contact distance of Mg − Mg reduced from ~3.1 Å at solid phase to ~2.4 Å at liquid which is comparable with the contact distance of Sb − Mg (~2.25 Å) at liquid. Moreover, the shoulder just after the principal peak of $g_{SbMg}(r)$ occurs at about 3.1 Å at solid state which corresponds the experimental Sb − Mg distance of 3.111 Å of 3 Mg ions around a Sb ion [17]. Radial distribution function of liquid Mg_3Sb_2 from MD and HNC calculations are also compared (Online Resource 3) which are in good agreement.

The running coordination number (RCN) $n_{ij}(r)$ is calculated from

$$n_{ij}(r) = 4\pi\rho_j \int_0^r r^2 g_{ij}(r)dr \tag{5}$$

and displayed in the Fig. 2 as an inset for 300 K and 1550 K. The number density of j ions is ρ_j. Solid-like and liquid-like behavior of the particles is evident from the stepwise and relatively continuous feature of the RCN, respectively. The position of the plateaus $n_{ij}(r)$ corresponds to the minimums in the radial distribution functions. The first three peaks of Mg − Mg pairs in solid dissolve into a single first peak in liquid with the RCN reducing from 24 to 20, respectively. $n_{Sb-Mg}(r)$ is estimated as 4 from the principal peak of Sb − Mg. The Sb − Mg first peak containing the shoulder as well gives the RCN as $n_{Sb-Mg}(r) = 7$ in solid which does not change upon melting. The $n_{Sb-Sb}(r)$ is calculated as 12 in the solid phase which also does not change during the melting.

Experimental partial structure factors $S_{ij}(k)$ can be extracted from three independently measured intensity $I(k)$. A way to define the $S_{ij}(k)$ is proposed by Faber and Ziman (FZ) to describe structural organization of ionic species in reciprocal space. The FZ partial structure factors are related to the distribution functions in real space through the Fourier transformation

$$S_{ij}(k) - 1 = \frac{4\pi\rho}{k} \int_0^r r\left[g_{ij}(r) - 1\right] sin(kr)dr \tag{6}$$

The $S_{ij}(k)$ of Mg_3Sb_2 at 1550 K is shown in Fig. 3a. The principal peak occurs at about k = 1.75 $Å^{-1}$ which corresponds to the extended-range order in real space reflecting the decaying character of the radial distribution. Structure factors were also calculated from MD by Fourier transform of the radial distribution functions and compared with HNC results (Online Resource 4). Beside the FZ structure factors that describe the ordering of the chemical species, the so called Bhatia-Thornton (BT) partial structure factors $S_{NN}(k)$, $S_{CC}(k)$ and $S_{NC}(k)$ characterize the global structure of the species regardless of their chemistry, the ordering of the species with respect to the sites and the short range relative order of the chemical species from Coulomb interactions, respectively.

The BT partial structure factors can be expressed in terms of the FZ structure factors [18]. $S_{NN}(k)$, $S_{CC}(k)$ and $S_{NC}(k)$ are particle density, concentration and particle density-concentration functions respectively.

$$\begin{aligned} S_{NN}(k) &= c_1^2 S_{11}(k) + c_2^2 S_{22}(k) + 2c_1c_2S_{12}(k) \\ S_{CC}(k) &= c_1c_2[1 + c_1c_2\{S_{11}(k) + S_{22}(k) - 2S_{12}(k)\}] \\ S_{NC}(k) &= c_1c_2[c_1\{S_{11}(k) - S_{12}(k)\} - c_2\{S_{22}(k) - S_{12}(k)\}] \end{aligned} \tag{7}$$

$S_{NN}(k)$, $S_{CC}(k)$ and $S_{NC}(k)$ are presented in Fig. 3b for molten Mg_3Sb_2 at T = 1550K. It has been verified numerically by Gillan [12] and Abernethy-Gillan [13] that in the case of $S_{CC}(k)$ approaches zero as $k \to 0$, $\lim_{k\to 0} S_{CC}(k) = 0$ (see Fig. 3b). For a liquid mixture, the criterion that the $S_{NN}(k)$ in the

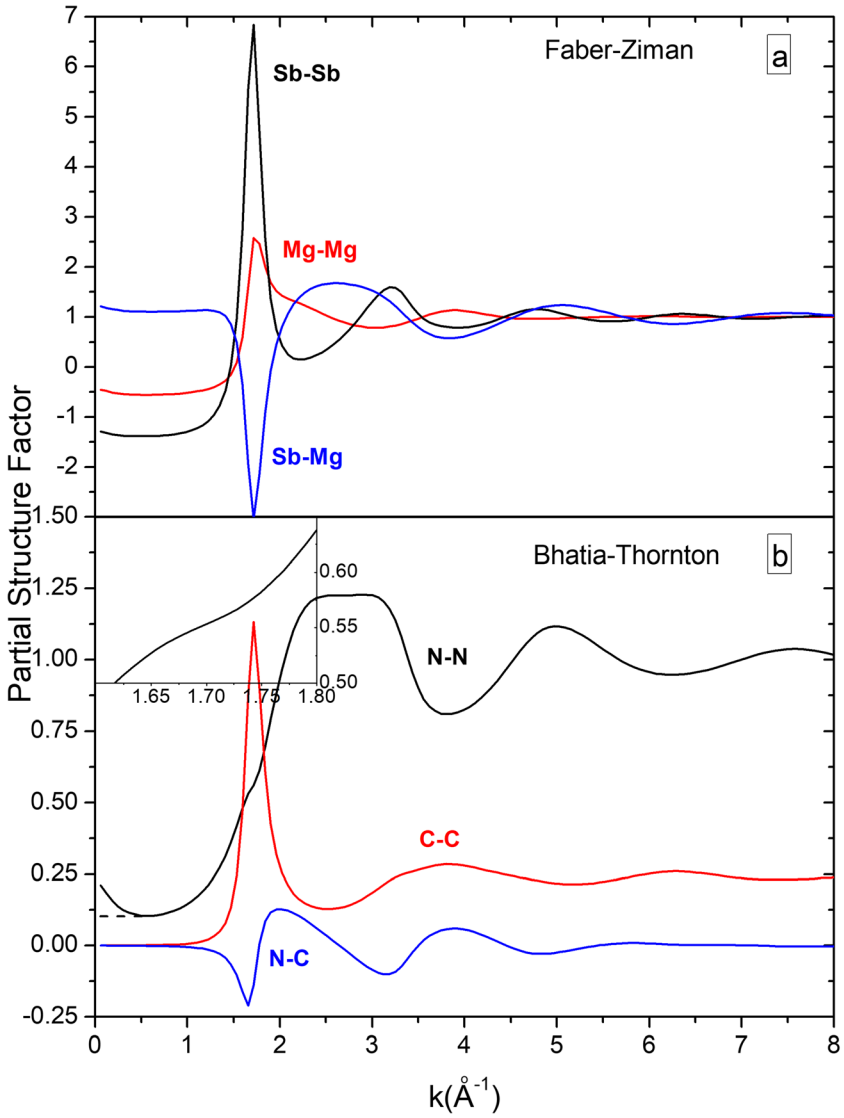


Fig. 3 The partial structure factors **a** Faber-Ziman **b** Bhatia-Thornton of molten Mg_3Sb_2 at T = 1550 K from the HNC theory. The inset shows the number-number (N-N) structure factor in the low-k region for $\Delta k = 0.01 A^{-1}$. 203 × 279 mm (300 × 300 DPI)

long wavelength limit $\left(\lim_{k\to 0} S_{NN}(k) > 0\right)$ must be positive is taken as an indicator of a physically significant calculation. The following equation relates this criterion to the isothermal compressibility.

$$\lim_{k\to 0} S_{NN}(k) = \rho k_B T K_T \tag{8}$$

The isothermal compressibility at 1550 K has been estimated as $K_T = \frac{S_{NN}(k\to 0)}{\rho k_B T} \cong 0.06717 \mathrm{GPa}^{-1}$ from the asymptotic line drawn parallel to *k*-axis which is acceptable for an ionic liquid within the limitations of the calculations. Compressibility at $T = 0$ is also obtained with GULP [16] program via static calculation method by using the same interaction potential and it is $0.02051 GPa^{-1}$.

Recently, topological structure of UO_2 had been examined in terms of pre-peak occurring at low-*k* in $S_{NN}(k)$. It was suggested that the origin of the pre-peak in $S_{NN}(k)$ displayed clusters composed of 3-, 4- and 5-fold Voronoi polyhedra [19]. Although it is not distinct as in UO_2, a small plateauing on the left half of the principal peak in $S_{NN}(k)$, shown as a magnified inset in Figure 3b, may be an indicator of the tendency of a low-*k* peak which has occurred at about $k \cong 1.7 \text{Å}^{-1}$. It had been pointed out that the $S_{NN}(k)$ is strongly influenced by the principal peak in $S_{UU}(k)$ (Uranium-Uranium structure factor) in low-k region [19]. Analogously, in the present calculations, the main peak in $S_{SbSb}(k)$ influences the $S_{NN}(k)$ where Sb being the negative ion. It should be specified that the anion (oxygen) is the more mobile ion for UO_2 while for Mg_3Sb_2 the cation (magnesium) is the more mobile. Consequently, generally speaking, the FZ structure factor of the less mobile ion influences the behaviour of the $S_{NN}(k)$ in the low-k region, which is irrespective of the type of the ion. Another result is that the pre-peak in the low-k region can be considered to be

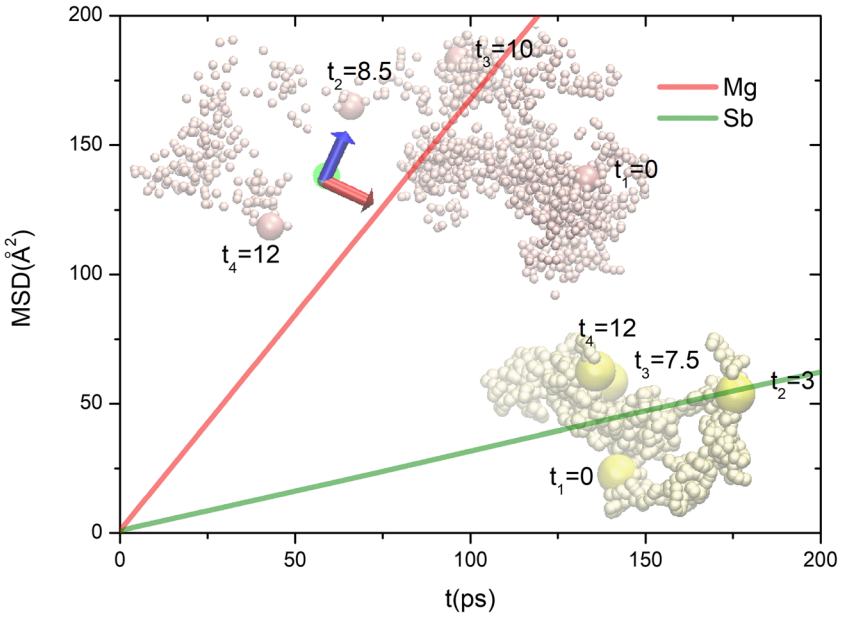


Fig. 4 Mean square displacement of Mg and Sb ions at melt from MD simulation calculations. Trajectories of each ion are shown for 12 ps. Large spheres are the snapshot of ions for four different instants. 291 × 203 mm (300 × 300 DPI)

evidence of an existence of a n-fold Voronoi polyhedra. However, the presence of mobile magnesium ions prevents the predomination of a single type of polyhedral [19]. In addition, intermediate range ordering stemming from the tetrahedral network structure is also reflected as a pre-peak around $k = 1.6\ \text{Å}^{-1}$ in the Ashcroft-Langreth or Faber-Ziman partial structure factor of more mobile ions is the systems such as SiO_2 and GeO_2 [20].

The molten metals require very high temperature to maintain a stable liquid state, which makes the diffusion coefficient difficult to measure due to the fluctuations in temperature that induces the convection and increases the mobility of the atomic species. The molecular dynamic simulation is a useful tool in order to estimate the diffusion coefficient at liquid phase. The molten magnesium antimony is one of the immiscible liquid compositions and used as electrodes in ambipolar electrolysis cell [21]. Information on ionic diffusion in liquid metal batteries is of importance in order to optimize the kinetic performance of the battery. The diffusion coefficient D_i can be calculated from mean-square displacement (MSD) of corresponding ionic species from the 12 × 12 × 12 MD supercell by the following relation,

$$D_i = \lim_{t\to\infty} \frac{1}{6t} \langle |r_i(t) - r_i(0)| \rangle \tag{9}$$

where $\langle |r_i(t) - r_i(0)| \rangle$ is the mean-square displacement. Figure 4 illustrates the MSD's of magnesium and antimony at 1550 K. The linear increase of MSD indicates the diffusive behaviour of both ionic components. From the slope of the MSD's (time interval 0-50 ps), the estimated diffusion coefficients are $D_{Mg} = 2.778 \times 10^{-5} cm^2 s^{-1}$ and $D_{Sb} = 0.507 \times 10^{-5} cm^2 s^{-1}$. The trajectories for 12 ps period for each ion, which is also inserted in Fig. 4, clearly show the difference between the thermally induced diffusion of the Mg and Sb ions. The radii of Mg and Sb are comparable [22] whereas the atomic mass of the antimony is about five times larger than that of magnesium ($M_{Mg} = 24.31\ g/mol$, $M_{Sb} = 121.76\ g/mol$). In addition to large difference in mass, the effective charge of the Sb ion $Z_{\text{Sb}} = -1.983588e$ is also larger than Mg ion $Z_{\text{Mg}} = 1.322392e$ which can be another reason for the large difference between the ionic constituents in binary salts. This suggests that not the size but the charge and mass of components is the determining factor for the ionic diffusion in molten Mg_3Sb_2.

Conclusions

Molten Mg_3Sb_2 is used in ambipolar electrolysis cell as electrodes. We have presented the ionic ordering and the transport results of integral equation calculations and molecular dynamics simulations using a semi-empirical potential for molten Mg_3Sb_2. We have estimated the liquid-state density at 1550 K as $\rho(T = 1550K) = 0.03722\ ions/\text{Å}^3 = 3.911\ g/ml$ from the minimum point of the total energy-density data of HNC calculations and $0.03504\ ion/\text{Å}^3 = 3.682\ g/ml$ from MD simulation, which is needed to be confirmed by the experiment to be acceptable for the future use. Antimony sublattice experiences relatively low degree of disordering upon melting while magnesium ions show larger mobility. The global structural analysis from Bhatia-Thornton structure factors manifests that the pre-peak, or the tendency in our case, occurring at low k-region in $S_{NN}(k)$ can be observed in the liquid systems related with ordering in real space. As a result, in liquid Mg_3Sb_2

intermediate range order is expected. Nevertheless, the presence of highly mobile magnesium ions in the liquid structure proves that there is not a single n-fold Voronoi polyhedral; it is the distribution of polyhedral clusters. It is possible to make inference from our current work and a previous study [19] that the pre-peak in $S_{NN}(k)$ can be observed in the systems whose ionic conductivity of the components are considerably different and is influenced by the pair structure factor of the less mobile ion. This is supported by the transport properties' calculations of MD simulation of molten Mg_3Sb_2. The diffusion coefficient of magnesium is estimated about three times higher than that of antimony. It is suggested that the mass of ionic components is the determining factor for the ionic diffusion in molten Mg_3Sb_2, not the size.

The interpretation and information on ordering and ionic diffusion of liquid magnesium antimonide provided by the present study, within the limitations of the liquid-state theories, could be useful for the future studies in order to optimize the performance of the liquid-state battery. Molecular dynamics simulation calculation results should be analyzed to uncover the distribution function of ordering in real space and to find most probable n-fold Voronoi polyhedra of molten Mg_3Sb_2. Nevertheless, these are in need of verification by experiment.

References

1. Barriga SA (2013) An electrochemical investigation of the chemical diffusivity in liquid metal alloys. Dissertation, Massachusetts Institute of Technology, Cambridge
2. Condron CL, Kauzlarich SM, Gascoin F, Snyder GJ (2006) Thermoelectric properties and microstructure of Mg_3Sb_2. J Solid State Chem 179(8):2252–2257. https://doi.org/10.1016/j.jssc.2006.01.034
3. Zhang KX, Qin XY, Xin HX, Li HJ, Zhang J (2009) Transport and thermoelectric properties of nanocrystal substitutional semiconductor alloys $(Mg_{1-x}Cd_x)_3Sb_2$ doped with Ag. J Alloys Compd 484(1–2):498–504. https://doi.org/10.1016/j.jallcom.2009.04.130
4. Xin HX, Qin XY, Jia JH, Song CJ, Zhang KX, Zhang J (2009) Thermoelectric properties of nanocrystalline $(Mg_{1-x}Zn_x)_3Sb_2$ isostructural solid solutions fabricated by mechanical alloying. J Phys D Appl Phys 42(16):165403–165412. https://doi.org/10.1088/0022-3727/42/16/165403
5. Bradwell DJ, Kim H, Sirk AHC, Sadoway DR (2012) Magnesium-antimony liquid metal battery for stationary energy storage. J Am Chem Soc 134(4):1895–1897. https://doi.org/10.1021/ja209759s
6. Tani J, Takahashi M, Kido H (2010) Lattice dynamics and elastic properties of Mg_3As_2 and Mg_3Sb_2 compounds from first-principles calculations. Phys B Condens Matter 405(19):4219–4225. https://doi.org/10.1016/j.physb.2010.07.014
7. Imai Y, Watanabe A (2006) Electronic structures of Mg_3Pn_2 (Pn=N, P, As, Sb and Bi) and Ca_3N_2 calculated by a first-principle pseudopotential method. J Mater Sci 41(8):2435–2441. https://doi.org/10.1007/s10853-006-5181-3
8. Ganeshan S, Shang SL, Zhang H, Wang Y, Mantina M, Liu ZK (2009) Elastic constants of binary Mg compounds from first-principles calculations. Intermetallics 17(5):313–318. https://doi.org/10.1016/j.intermet.2008.11.005
9. Zhou DW, Liu JS, Xu SH, Peng P (2010) Thermal stability and elastic properties of Mg_3Sb_2 and Mg_3Bi_2 phases from first-principles calculations. Phys B Condens Matter 405(13):2863–2868. https://doi.org/10.1016/j.physb.2010.04.013
10. Günay SD (2016) Calculations of thermophysical properties of magnesium antimonide (α-Mg_3Sb_2). Turk J Phys 40(3):264–269. https://doi.org/10.3906/fiz-1601-15
11. Hansen JP, McDonald IR (1986) The theory of simple liquids. Academic, New York
12. Gillan MJ (1979) A new method of solving the liquid structure integral equations. Mol Phys 38(6):1781–1794. https://doi.org/10.1080/00268977900102861
13. Abernethy GM, Gillan MJ (1980) A new method of solving the HNC equation for ionic liquids. Mol Phys 39(4):839–847. https://doi.org/10.1080/00268978000100721
14. Refson K (2000) A portable molecular dynamics simulation program for serial and parallel computers. Comput Phys Commun 126(3):310–329. https://doi.org/10.1016/S0010-4655(99)00496-8
15. Fumi FG, Tosi MP (1964) Ionic sizes and born repulsive parameters in the NaCl-type alkali halides—I: the Huggins-Mayer and Pauling forms. J Phys Chem Solids 25(1):31–43. https://doi.org/10.1016/0022-3697(64)90159-3
16. Gale JD, Rohl AL (2003) The general utility lattice program (GULP). Mol Simul 29(5):291–341. https://doi.org/10.1080/0892702031000104887
17. Martinez-Ripoll M, Haase A, Brauer G (1974) The crystal structure of α-Mg_3Sb_2. Acta Crystallogr B 30:2006–2009. https://doi.org/10.1107/S0567740874006285
18. Waseda Y (1980) The structure of non crystalline materials: liquids and amorphous solids. McGraw-Hill, London
19. Benmore CJ, Skinner LB, Lee B, Weber JKR, Parise JB, Williamson M (2016) Topological ordering in liquid UO_2. J Phys Condens Matter 28(1):015102–015107. https://doi.org/10.1088/0953-8984/28/1/015102
20. Hawlitzky M, Horbach J, Binder K (2004) Computer simulations of SiO_2 and GeO_2. In: Attinger S, Koumoutsakos P (eds) Multiscale Modelling and Simulation, Lecture Notes in Computational Science and Engineering, vol 39. Springer, Berlin, pp 187–193
21. Kim H, Boysen DA, Newhouse JM, Spatocco BL, Chung B, Burke PJ, Bradwell DJ, Jiang K, Tomaszowska AA, Wang K, Wei W, Ortiz LA, Barriga SA, Poizeau SM, Sadoway DR (2013) Liquid metal batteries: past, present, and future. Chem Rev 113(3):2075–2099. https://doi.org/10.1021/cr300205k
22. Kittel C (2005) Introduction to solid state physics. Wiley, Hoboken